Tellus (2001), 53B, 344–358
Printed in UK. All rights reserved

TELLUS
ISSN 0280–6509

Physical characterization of aerosol particles during nucleation events

By PASI AALTO[1,*], KAARLE HÄMERI[1], EDO BECKER[2], RODNEY WEBER[3], JAAN SALM[4], JYRKI M. MÄKELÄ[1], CLAUDIA HOELL[2], COLIN D. O'DOWD[1,2], HANS KARLSSON[5], HANS-CHRISTEN HANSSON[5], MINNA VÄKEVÄ[1], ISMO K. KOPONEN[1], GINTAUTAS BUZORIUS[1] and MARKKU KULMALA[1], [1]*Department of Physics, PO Box 9, FIN-00014, University of Helsinki, Finland;* [2]*University of Sunderland, Centre for Marine and Atmospheric Sciences, School of the Environments, Benedict Building, St. George's Way, Sunderland SR2 7BW, UK;* [3]*School of Earth and Atmospheric Sciences, Georgia Institute of Technology, Atlanta, GA 30332-0340, USA;* [4]*Institute of Environmental Physics, University of Tartu, Ülikooli 18, 50090, Tartu, Estonia;* [5]*Institute of Applied Environmental Research, Stockholm University, SE-10691, Stockholm, Sweden*

(Manuscript received 10 May 2000; in final form 22 January 2001)

ABSTRACT

Particle concentrations and size distributions have been measured from different heights inside and above a boreal forest during three BIOFOR campaigns (14 April–22 May 1998, 27 July–21 August 1998 and 20 March–24 April 1999) in Hyytiälä, Finland. Typically, the shape of the background distribution inside the forest exhibited 2 dominant modes: a fine or Aitken mode with a geometric number mean diameter of 44 nm and a mean concentration of 1160 cm^{-3} and an accumulation mode with mean diameter of 154 nm and a mean concentration of 830 cm^{-3}. A coarse mode was also present, extending up to sizes of 20 μm having a number concentration of 1.2 cm^{-3}, volume mean diameter of 2.0 μm and a geometric standard deviation of 1.9. Aerosol humidity was lower than 50% during the measurements. Particle production was observed on many days, typically occurring in the late morning. Under these periods of new particle production, a nucleation mode was observed to form at diameter of the order of 3 nm and, on most occasions, this mode was observed to grow into Aitken mode sizes over the course of a day. Total concentrations ranged from 410–45 000 cm^{-3}, the highest concentrations occurring on particle production days. A clear gradient was observed between particle concentrations encountered below the forest canopy and those above, with significantly lower concentrations occurring within the canopy. Above the canopy, a slight gradient was observed between 18 m and 67 m, with at maximum 5% higher concentration observed at 67 m during the strongest concentration increases.

1. Introduction

Aerosol particle formation events in tropospheric air have been observed to occur in different environments around the world. Recent observations of new particle production have been reported, for example, in the free troposphere (Weber et al., 1999), the marine boundary layer (Covert et al., 1992), coastal sites (O'Dowd et al., 1999), the Arctic (Pirjola et al., 1998; Wiedensohler et al, 1996), the Antarctic (O'Dowd et al., 1997) and over boreal forests (Mäkelä et al., 1997). Bursts of charged nanometer particles have been observed also during regular measurements of air ions (Hõrrak et al., 1998). In most of these cases,

* Corresponding author.
e-mail: pasi.p.aalto@helsinki.fi

nucleation mode ($d < 10$ nm) particles have been observed to grow into radiatively-active particle ($d > 100$ nm) sizes with the potential to enhance both the scattering efficiency of the aerosol and its cloud nucleating properties.

While there have been many observations of new particle production, there have been few co-ordinated efforts to study background new particle production until recently. One of these dedicated experiments, BIOFOR (Biogenic Aerosol Formation Over the Boreal Forest), was conducted in Hyytiälä, Southern Finland over a 2-year period, comprising continuous aerosol measurements and 3 intensive field experiments to examine the influence of meteorology and biogenic organic emissions on aerosol formation (Kulmala et al., 2001). During the BIOFOR campaigns, one objective was to measure the concentration and size distribution of the newly-formed particles with as high an accuracy as possible both inside and above the forest. The profile measurements were aimed at determining whether the forest behaves as a source or a sink for small particles and to see whether aerosol growth rates differ within and above the canopy. This article describes the aerosol measurement systems used, instrument calibrations and summarises the problems and difficulties encountered in trying to achieve the aerosol measurement objectives during the campaign. The primary objective of this study is to report aerosol characteristics and parameters associated with new particle production events.

2. Measurement system

Unless otherwise mentioned, all the data presented in this paper is from the BIOFOR 3 period (20 March–24 April 1999). Similarly the description of the measurement system is focused to this period. The reason for this is that most of the nucleation events were detected during this period and the instrumentation as well as calibrations and various tests were more developed and complete during the period. Fig. 1 shows the measurement site, instruments used during the spring 1999 campaign and their placement. Sampling was conducted from three different levels at heights of 2, 18 and 67 m, respectively. Instruments were located in 4 different places on the site: the cottage, the mast, the truck and the cottage of Tapiola.

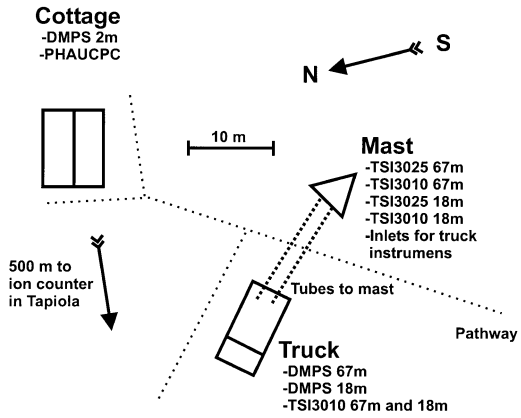

Fig. 1. Drawing of the measurement site.

More detailed description about Hyytiälä measurement station is presented in this issue (Kulmala et al., 2001).

Main Cottage. The lowest measurement level sampling was conducted in the cottage where the sample was taken from a 2-m height inside the forest. The primary sample tube was about a meter long, 5 cm in inner diameter and the flow rate through the tube was 2.5 $m^3\ h^{-1}$. From the primary flow, sample flow was drawn to the instruments with a short, 8 mm diameter tubing.

Mast and truck. The secondary measurement point was the mast. Sampling was conducted from 18-m and 67-m levels in the mast through sampling lines leading to the truck. The sample lines to these points above the forest were 23.7 mm stainless steel tubing. The total lengths of the lines were 30 m and 82 m. The flow rate inside these lines was 25 LPM. We had instruments also up in the mast with short sample lines.

Tapiola cottage. Additionally an extra measurement location was used at a distance of a few hundred meters away from the primary site in the Tapiola cottage. Samples on this site were also taken inside the forest from the height of 2 m.

2.1. Instrumentation

The total concentration of aerosol particles was measured with two different particle counters (CPC). The first one was TSI model 3010 (Quant et al., 1992), which measures particles at sizes starting from approximately 10 nm up to 3 μm. The maximum concentration which this device

can measure is 10 000 cm^{-3}. The second counter type was TSI model 3025 (Stolzenburg and McMurry, 1991). This device can measure smaller particles and higher concentrations. The minimum particle diameter is less than 3 nm and highest concentration 100 000 cm^{-3}. By comparing the total concentrations given by these counters, ultrafine particle (from 3 nm to 10 nm) concentration can be determined. During BIOFOR, two CPC pairs consisting of one TSI 3010 and one TSI 3025 were used. The concentrations were logged at 10 Hz, however, later analysis determined that the frequency response of the CPCs was between 0.5–1 Hz. The CPC pairs were placed in heated chambers on the mast at levels of 18 and 67 m in order to avoid excessive sampling losses through long sample tubes. The sampling lines used for these CPCs were identical with a length of 20 cm and 4 mm in diameter. Additionally, 2 TSI model 3010 particle counters, located in the truck, sampled from 18-m and 67-m levels through the long sampling lines, however, this data was used more for general monitoring and quality control reasons.

For the detection of the recently-formed particles, an additional pulse height analysis ultrafine condensation particle counter (PHAUCPC) was used sampling from inside the cottage (Saros et al., 1996). This device is similar to the TSI model 3025 with the same lower cut-off diameter but an alternative light source, however, it is not able to measure as high concentrations as the standard TSI 3025. The alternative light source allows unique pulse height detection and counting, leading to the a particle sizing capability between 3 and 10 nm. With this instrument, measurements of both the total concentration and the ultrafine particle concentration were conduced simultaneously using a single device.

For sub-micron particle sizing, the main instrument used was the differential mobility particle sizer (DMPS) and 3 systems were located at different levels. The first one is used in the long-term studies and is located in the cottage measuring aerosol properties from within the forest canopy. This system contained two DMPS devices: the first device classified the particles between 3 and 10 nm and the second device classified between 10 nm and maximum 500 nm. Both devices used Hauke-type differential mobility analyzer (DMA) (Winklmayr et al., 1991) and closed loop sheath flow arrangement (Jokinen and Mäkelä, 1997). The 1st device had a 10.9-cm long DMA and second device a 28-cm long DMA. Before sizing aerosol was neutralized with a 2mCi Krypton-85 beta source. The particle counter of the 1st device was TSI model 3025 and the 2nd device had TSI model 3010. The 2nd DMPS system had one Hauke-type DMA with a length of 10.9 cm, TSI model 3010 particle counter, closed loop sheath flow arrangement and Krypton-85 aerosol neutralizer. It measured size distribution for particles beginning from 10 nm up to 500 nm. This device was sampling from 18-m level. The 3rd DMPS system was identical to the long-term study system and was measuring particle size distribution above the forest from the 67-m level from 3 to 850 nm in diameter. The 18-m level and 67-m level DMPSs were placed in the truck. The 2-m level and the 67-m level DMPS had a measurement period of 10 min. With the 18-m level, the DMPS period was around 15 min. The sheath air flows of 18-m and 67-m level DMPSs were dried, but the 2-m DMPS sheath flow was not dried.

For large-particle sizing, an aerodynamical particle sizer (APS), TSI model 3320 was used to measure size distributions from 0.7 μm up to 20 μm. This instrument had its own sampling line of the 2-m level inside the forest and was located in the truck. The sample flow of the APS was not dried.

Small or cluster ions are generated in the atmosphere by cosmic radiation and natural radioactivity (Israël, 1970). Cluster ions are subsequently formed via ion-molecule reactions in the atmosphere before they obtain their final size (Mohnen, 1977; Luts and Salm, 1994). Certain thermodynamical causes limit the growth of small ions at a mobility of 0.5 $cm^2\ V^{-1}\ s^{-1}$ (1.6 nm) in ordinary conditions. Recent investigations have shown that the range of intermediate ions extends from 0.034 to 0.5 $cm^2\ V^{-1}\ s^{-1}$, i.e. from 1.6 to 7.4 nm (Hõrrak et al., 2000). Ions larger than this are called light large ions. The simplest apparatus for measuring air ions is the integral counter (Tammet, 1970). In order to estimate the concentrations of charged nanometer particles, 4 integral air ion counters, switched to positive polarity, were operating in Tapiola from 31 March to 29 April 1999. The common air inlet was at a height of 2 m above the ground. The limiting mobilities of the counters

were set to 0.02, 0.063, 0.2, and 0.64 $cm^2\ V^{-1}\ s^{-1}$. The output signals of the counters were saved as average values for 10-min intervals. The 4, partly-overlapping mobility ranges can be used to derive ionic concentrations in 3 different mobility classes, namely small, intermediate and light large ions. Air ion measurements represent a method for the measurement of aerosol particles (Hõrrak et al., 1998). From the aerosol point of view, the intermediate ions are comparable to charged aerosol particles in the size range of 1.9–7.4 nm. Furthermore, the light large ions may be interpreted as the charged fraction of aerosol particles above 7.4 nm in diameter.

During the 1998 campaigns (14 April–22 May 1998 and 27 July–21 August 1998), the DMPS systems were the same as during the 1999 campaigns. The DMPSs measuring at 18- and 67-m levels above the forest were just placed vice versa. The instrument measuring from 3-nm sizes was placed on the 18-m level and the instrument measuring from 10 nm was placed on the 67-m level. All the CPCs were placed in the truck and were measuring through the long sampling lines. During the 1998 campaigns, we didn't have APS, PHAUCPC or ion counter.

2.2. *Instrument calibration*

Before the campaign, all the particle counters in the CPC pairs and the DMPS systems were calibrated. Also, the losses inside the DMAs were determined. The calibration procedure was as follows: silver particles were produced with a tube furnace. The furnace temperature and flow rate through the furnace were adjusted to achieve suitable particle size distributions for calibration purposes. The silver aerosol was classified with a Hauke-type DMA and this monodisperse aerosol concentration was measured with an electrometer (TSI model 3068 A). The concentration measured with the device under calibration was compared to the electrometer reading. Calibrations of all the TSI model 3025 particle counters were determined this way. After this, one calibrated 3025 counter was selected to be a reference for all the TSI model 3010 particle counters because the sensitivity of the electrometer is not sufficient for calibration of these counters. The DMA losses were determined the same way by comparing the total concentration measured with a DMPS to the electrometer reading. This test was done with charged aerosol. Neutralizer was not used before the DMA. Fig. 2 shows the calibration curves of the particle counters used in the 2-m DMPS system. Calibration curves seem to resemble the calibration found from literature (Wiedensohler et al., 1997). The TSI model 3025 cut size is below 3 nm and the TSI model 3010 around 6 nm with temperature difference of 25°C between saturator and condenser. The PHAUCPC was calibrated the same way as the TSI 3025, with the exception that pulse height distributions were also recorded. This calibration agreed very well with previous, more extensive tests.

Fig. 3 shows the result from the DMA sampling loss calibration. These DMAs were used in the

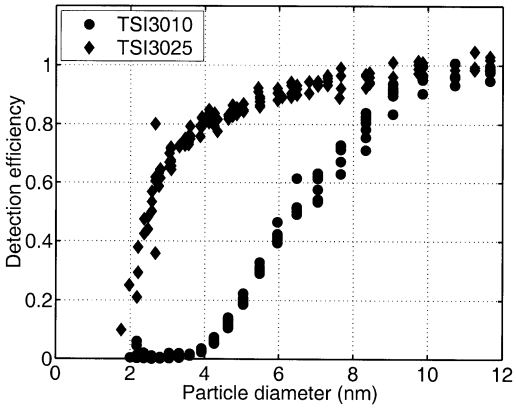

Fig. 2. Calibration of CPCs in the 2-m DMPS system.

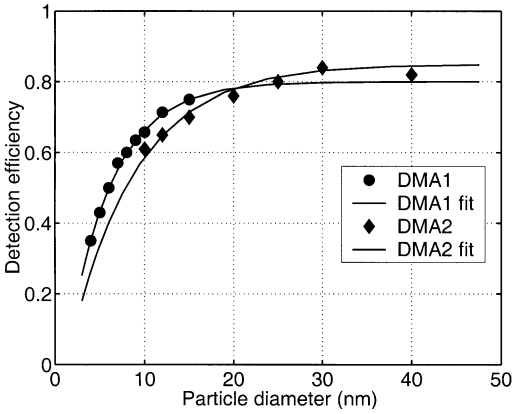

Fig. 3. Calibration of DMAs in the 2-m DMPS system. DMA1 is the 10.9 cm long and DMA2 the 28 cm long DMA.

2-m DMPS system. Curves seem to behave as expected except that they don't reach the value of unity even with large particle diameters. The same behaviour has been reported in the literature (Birmili et al., 1997). The reason for this is unknown, but most likely, the DMAs are manufactured poorly and some critical dimensions are not what they should be. However we believe that this behaviour was consistent and can be corrected according to calibration.

One problem with the measurements was the high sampling losses caused by the long sampling tubes used with above the forest sampling points. We found that diffusional loss equations of normal laminar flow were not valid for our sampling line. Because of this, we measured the losses by producing monodisperse silver aerosol and measuring its concentration before and after the tube. It was noticed that between 30 and 35 LPM, the flow becomes turbulent with a Reynolds number around 2000. Thus, a 25 LPM sample flow was selected to avoid turbulence (Fig. 4). Measurements can be modeled with normal laminar flow diffusion loss equations by multiplying the actual tube length with a factor of 1.7. The reason for this behaviour is unknown. Obviously, the flow pattern inside the tube is not ideal, which increases the losses. This calibration is taken into account when DMPS measurements were inverted.

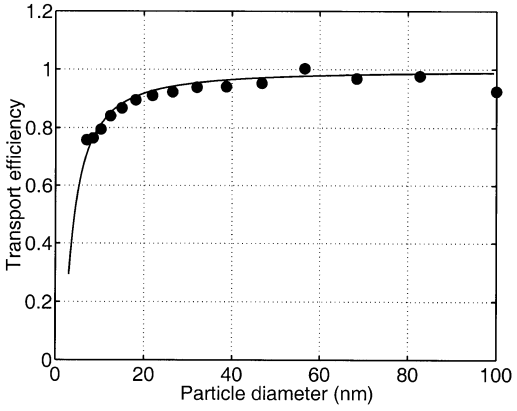

Fig. 4. Calibration of losses in a steel tube with length of 37.5 m, diameter 23.7 mm and aerosol flowrate of 25 LPM.

2.3. Data analysis

All the concentrations were corrected to STP conditions (273.15 K, 1013.25 hPa). The time used during the campaign is the Finnish winter time (UTC + 2 h).

The DMPS measurements were inverted using normal pseudo inversion routine with DMA kernels by Stolzenburg (1988), and the CPC detection efficiencies according to the calibration and charging probabilities of Wiedensohler (1988). Sampling line losses and losses inside the DMAs were taken into account. Inverted particle size distributions were fitted using 3 log-normal distributions. Detection limits for 2-m and 67-m DMPS systems are plotted in Fig. 5. One can see from the figure that 67-m DMPS has very high detection limit when particles are smaller that 5 nm due to sampling losses. During the campaign, we detected practically no particles smaller that 5 nm with 67-m DMPS. For the 2-m DMPS system, the situtation is better. The statistical error of concentration of particles smaller than 5 nm is roughly 30% with typical concentrations measured, and for particles between 5 and 10 nm in diameter, 10%.

From the PHAUCPC pulse height distributions, the total concentration was integrated and small-particle concentrations were calculated by integrating the distribution from the 1st channel to a certain, calibration-determined channel, to get an estimate of the particle concentration below 10, 6, 5 and 4 nm in diameter. The detection limit was about 2.7 nm in diameter. For all the CPCs, the

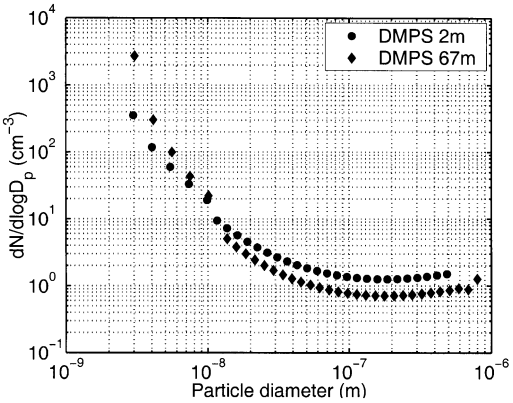

Fig. 5. Detection limits of the 2-m and 67-m DMPS systems.

statistical error of total concentration with 1-min integration time was less than 1%. For all ultrafine particle counters, the uncertainty of flow rate is much larger, around 5%.

The large-particle size distributions measured with the APS were shifted to mobility diameter by dividing the aerodynamic diameter by the square root of the estimated particle density 1.9 g cm^{-3}. This density is not based on the actual measurements. We found that this density gives the best overlap between DMPS and APS size distributions.

Due to the nature of integral ion counter, the concentrations can be calculated by means of a special inversion algorithm (Tammet, 1970). It is expedient to use 3 fractions, determined according to Table 1. The boundary of 20 nm cannot be exactly determined, since the larger the particle, the smaller its contribution to signal is.

2.4. *Known problems with the instrumentation*

During the measurement campaigns, the CPC pairs were placed on the mast to minimize the sampling losses. With the TSI model 3025, this succeeded quite well but the TSI model 3010 experienced some difficulties. Due to temperature variations in the environment, concentrations sometimes dropped drastically compared to TSI model 3025 on 6 different days. Temperature variations were mostly caused by the cheap thermostat controlling the temperature of the CPC chambers. A thermostat with more logic should have been used. Additionally there were some problems with the system used to read the TSI model 3010 concentration. It seems that during high concentration episodes, the concentration can be seriously underestimated. These 2 problems were impossible to correct. They became dominant after 10 April and this data was therefore omitted from the analysis. All the particle counters had also some drift in flow rates, which were corrected by inter-comparing their concentration during days when mixing was strong and no small particles existed.

The PHAUCPC also experienced some problems during the Spring 1999 period. It worked during the 1st week in April, but after that, the light source of the particle detector failed. The instrument was serviced, however; this took 1 week of active campaign time. The instrument was back online during the last week and a half of the campaign.

The DMPS systems measuring above the forest also had problems because of the long sampling lines; however, it is difficult to take the sampling losses into account. This can be seen by comparing CPC pair and DMPS total concentrations during the small-particle events. Therefore, concentrations between different instruments are not comparable when small particles are present due to enhanced losses at these sizes. The sampling lines for the 67- and 18-m DMPS systems should have been shorter, but that would have been logistically quite difficult to achieve. The particle counter in the 18-m level DMPS system experienced severe instability during the campaign. We were able to correct the problem during the campaign but the data before 14 April is not regarded as usable. The working days of different instruments are listed in Table 2.

The ion counter was logistically placed 500 m apart from the main group intruments. The main problems in interpreting the ion measurements, however, arise from the fact that the ion counters measure only charged particles. All comparisons with the aerosol instruments rely purely on the assumption of the ambient steady state charging

Table 1. *Air ion fractions*

Fraction	Symbol	Mobility ($cm^2\ V^{-1}\ s^{-1}$)	Diameter (nm)
small ions	*n*	0.35–∞	0–1.9
intermediate ions	*m*	0.035–0.35	1.9–7.4
light large ions	*N*	ca. 0.005–0.035	7.4–ca. 20

Table 2. *Working days of the different instruments excluding breaks shorter than half a day*

Instrument	Working days
TSI 3010 18 m	20 March–10 April
TSI 3025 18 m	20 March–24 April
TSI 3010 67 m	20 March–10 April
TSI 3025 67 m	20 March–24 April
PHAUCPC	1 April–6 April, 13 April–29 April
DMPS 2 m	continuous
DMPS 18 m	14 April–27 April
DMPS 67 m	19 March–27 April
APS	25 March–26 April
ion counters	31 March–23 April, 24 April–29 April

conditions. Secondly, the instrument functions of the integral counters have long tails towards larger ion sizes. Since the charging state of the aerosol is not known in detail, the comparisons remain qualitative.

3. Results and discussion

3.1. Aerosol statistics

Particle number concentration statistics over the BIOFOR 3 measurement period for all the instruments over their working days are presented in Table 3. The average particle number concentration of particles larger than 3 nm (TSI 3025) was close to 4900 cm^{-3} and larger than 10 nm (TSI 3010) 3700 cm^{-3}. The values integrated from the DMPS measurements are lower than the values detected with TSI 3010. The concentration was generally higher during the periods when particle production rates were high and lower during cloudy periods. The air mass origin didn't influence the total particle concentration significantly. In continental air masses, concentrations were about the same as in marine air masses with number concentration values ranging over 2 orders of magnitude from 410 to 45 000 cm^{-3}. The higher accumulation mode particle concentration in continental air masses compensated the higher Aitken mode concentration in the marine air masses quite well, resulting in equalling total particle concentration. The highest concentrations occurred during the particle production events.

Particle surface area and the volume statistics from the height of 2 m are presented in Table 4. The surface area and volume are for dry particle sizes. Ambient aerosol surface area can be up to 3 times larger than dry surface area and volume 5 times higher, based on the hygroscopicity data (Hämeri et al., 2001). Mean particle dry surface area was close to 130 $\mu m^2\,cm^{-3}$ and volume 8.1 $\mu m^3\,cm^{-3}$. The variation in surface area was higher than in that of particle number. The lowest values were around 5.5 $\mu m^2\,cm^{-3}$ and the highest around 1000 $\mu m^2\,cm^{-3}$. Particle volume variation was less, with a minimum of 1 and maximum 43 $\mu m^3\,cm^{-3}$. For surface area, the difference between continental and marine air masses was quite clear. In southerly (continental) air masses during 27 and 28 March and after 16 April, the particle surface area was almost 10 times higher than in westerly or northerly (marine) air masses.

Statistics of the fitted DMPS particle size distributions from the height of 2 m for all BIOFOR periods are presented in Table 5. These values should not be considered to show typical behaviour of the modal parameters during the season. Variation of these parameters from year to year is quite strong. The nucleation mode was the most variable in all respects. Both concentration and mean diameter evolved during particle production episodes so much that it is meaningless to study average properties. However, both the Aitken and especially the accumulation mode had very well characterized properties. The Aitken mode mean concentration was 1160 cm^{-3} and mean diameter was 44 nm. For the accumulation mode, the mean concentration was lower 830 cm^{-3} and mean diameter 154 nm. Aitken mode concentrations were the highest during the sunny particle production periods. Accumulation mode concentration was the highest as was the particle surface area in southerly air masses.

Particle concentrations were measured from 3 different levels with similar ultrafine particle counters. Between 09:00 and 18:00, concentrations were

Table 3. *Particle concentration statistics (cm^{-3})*

Instrument	Mean	Min.	1st quartile	Median	3rd quartile	Max.
TSI 3010 18 m	3810	417	2100	3560	4990	13900
TSI 3025 18 m	4920	384	2490	3970	6050	43300
TSI 3010 67 m	3610	414	2000	3360	4860	11500
TSI 3025 67 m	4880	396	2440	3960	5950	44500
PHAUCPC 2 m	4870	743	2780	3960	6090	26900
DMPS 2 m	3440	310	1820	2880	4320	25400
DMPS 18 m	3300	890	2000	2670	4090	20600
DMPS 67 m	3110	321	1730	2710	3990	21100

Table 4. *Particle surface area and volume statistics calculated from DMPS (2 m level) and APS measurements; units are* $\mu m^2\ cm^{-3}$ *and* $\mu m^3\ cm^{-3}$

Variable	Mean	Minimum	1st quartile	Median	3rd quartile	Maximum
surface area	133	5.52	59.3	93.2	164.6	1036
volume	8.14	1.00	3.28	5.73	10.8	42.7

Table 5. *Statistics of fitted DMPS 2-m size distributions during all 3 BIOFOR periods*

Mode	Variable	Mean	Min.	1st quart.	Median	3rd quart.	Max.
nuc.	N (cm^{-3})	830	0	0	122	585	42400
	CMD (nm)	16.1	1.12	12.0	16.4	22.9	89.4
	GSD	1.52	1.00	1.39	1.48	1.61	4.14
Aitken	N (cm^{-3})	1159	0	378	845	1511	12825
	CMD (nm)	44.2	1.62	33.3	49.7	64.1	178
	GSD	1.64	1.00	1.46	1.58	1.74	23.4
acc.	N (cm^{-3})	830	0	232	427	954	33557
	CMD (nm)	154	1.81	126	156	194	532
	GSD	1.68	1.00	1.50	1.64	1.80	4.87
total	N (cm^{-3})	3100	310	1630	2630	3960	25400

very well correlated between different levels. Between the 18-m and 67-m levels, correlation calculated over 1 h was very close to 1, and between 18-m and 2-m levels, correlation was about 0.98. However during night time, the correlation was much lower. Between the 18-m and 67-m levels, the correlation coefficient was on average 0.8 and between the 18-m and 2-m levels, 0.9. It seems that mixing during the day time is very high above the forest canopy but less intense inside the canopy. During night time, different levels are very isolated because of the high stability. Lower correlations between the highest levels originate most likely due to very local pollution, which is able to reach the 2-m and 18-m levels but not the 67-m level.

3.2. *Particle production events*

Particle production events are quite common during the Spring in Hyytiälä (Mäkelä et al., 1997). The dates of particle production are listed in Tables 6, 7. In the tables, the start and stop time of the production and the maximum concentration of the nucleation mode particles are also presented. The particle number concentration, surface area and volume before the production event are presented in the last 3 columns. The start and stop times are determined from the 2-m DMPS data by investigating the concentration of particles smaller than 5 nm. The maximum nucleation mode concentration is determined from the fitted 2-m DMPS data; the particle concentration before the event is determined from the 67-m TSI 3025 data, and particle surface area and volume from the 2-m DMPS and APS data.

Events were seen during sunny days during the campaign and the presence of clouds seemed to suppress particle production very efficiently, perhaps due to lower photochemical activity. Particle production was not detected when global radiation was less than 400 $W\,m^{-2}$. During all the event days, particle surface area and volume were lower than the average. Particle production was not detected when particle surface area was higher than 100 $\mu m^2\ cm^{-3}$. Similar behaviour can be seen in Fig. 6 where average particle size distributions are plotted on event days and no-event days. During no-event days, the Aitken and accumulation mode concentrations are almost equal, but during event days, the accumulation mode concentration is lower and the Aitken mode concentration higher than during no-event days. For coarse particles, there is no difference between event and no-event days. It was also found that SO_2 and NH_3 were higher during the event days when the days with high surface area were neglected (Janson et al., 2001). Most often, the events started between

Table 6. *BIOFOR 1 event date data from 2-m measurements; existing concentration means total particle concentration just before the event*

Date	Start time	Stop time	Particles produced (cm^{-3})	Existing concentration (cm^{-3})
15 April	09:00	15:00	—	3560
16 April	09:00	13:40	—	4480
25 April	07:40	17:10	1680	3180
30 April	09:20	13:25	2477	5000
9 May	09:00	19:20	8630	2000
11 May	09:40	16:30	6530	1440
13 May	10:15	17:50	3400	1290
15 May	10:00	15:05	1190	1730
17 May	07:40	16:30	5740	3160
18 May	10:00	14:50	3350	2440
20 May	07:10	16:15	7920	997
21 May	08:30	13:50	2940	4330

Table 7. *BIOFOR 3-event date data from 2-m measurements; existing number concentration, surface area and volume indicate the values just before the event*

Date	Start time	Stop time	Particles produced (cm^{-3})	Existing concentration (cm^{-3})	Surface area ($\mu m^2\ cm^{-3}$)	Volume ($\mu m^3\ cm^{-3}$)
29 March	12:14	19:26	3100	6100	47	2.9
30 March	08:38	16:48	12300	6200	73	4.8
2 April	12:43	17:17	7200	1500	29.5	1.78
3 April	10:05	16:34	3800	3800	41.9	1.53
4 April	09:07	19:41	6500	2600	56.7	3.77
5 April	08:52	15:22	10800	3500	33.1	2.85
6 April	10:19	14:09	3100	5400	86.9	6.00
8 April	12:00	15:21	5500	1300	41.0	1.96
9 April	09:07	13:26	9500	5400	47.7	2.46
10 April	08:24	14:24	3000	1500	10.4	1.59
12 April	08:38	16:19	6100	3000	63.8	4.61
13 April	09:50	17:31	7500	3100	—	—
14 April	10:48	15:21	5200	2800	70.2	4.56
19 April	10:33	18:00	3400	3400	95.1	5.55
20 April	09:36	11:45	600	5100	—	—
21 April	13:12	15:50	1300	3400	91.9	5.02
27 April	08:09	12:57	33	—	—	—
29 April	06:57	17.45	4470	—	—	—

08:00 and 11:00, and finished between 15:00 and 18:00. During the days when events started later during the morning or afternoon, either global radiation was less than 400 $W\ m^{-2}$ or particle surface area was higher than 100 $\mu m^2\ cm^{-3}$ before the event.

In southern air masses, the produced small-particle concentrations were lower than in other types of air masses perhaps because of typically higher surface area and increased cloudiness compared to more northern air masses (Kulmala et al., 2000). The strongest events were seen when particle production started early in the morning in good conditions (low existing surface area and high radiation). An exception for this is the event during 2 April when strong events was seen even when small particles appeared just after noon. Fig. 7 shows this event as an example. The size distribution remains quite stable during the night and through the early morning. During the morn-

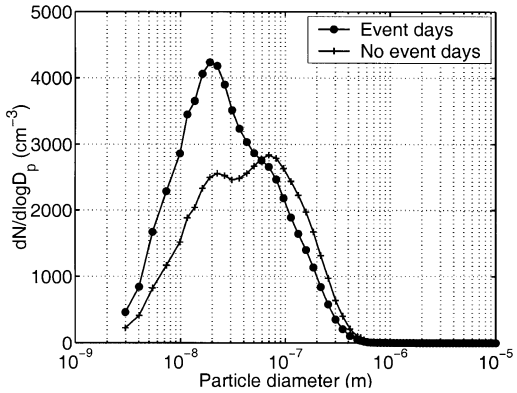

Fig. 6. Average particle number size distributions during event and no-event days.

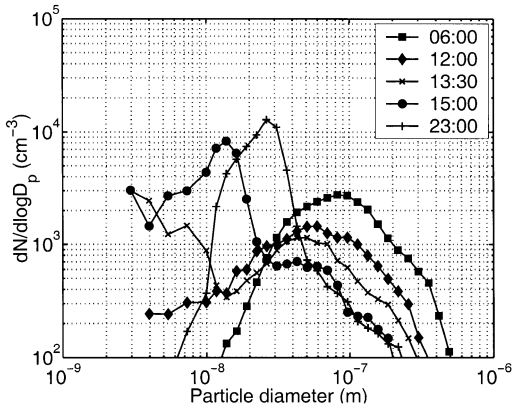

Fig. 7. Particle size distributions measured with DMPS at 2-m height during 2 April 1999.

ing and early afternoon, the concentration and mean diameter of the particle size distribution decreases. This reduction is due to the breakup of a stable nocturnal surface layer followed by vigorous mixing with the residual boundary layer, typically containing lower particle concentrations (Nilsson et al., 2001). Production of small particles continues through to 17:00; thereafter, the produced nucleation mode continues its growth into the next day. Between 14:00 and 15:00, the particle mean diameter changes quite rapidly by 7 nm. It seems possible that particle production has already started earlier, in more suitable conditions, and particles which have already grown to larger sizes are advected to sampling site. During the next 2 h, growth is about 3 nm/h. During the early evening growth stops, but continues after 21:00 with a growth rate of 4 nm/h. It is quite common that the growth of the nucleation mode particles stops sometimes during the afternoon and continues again later during the evening.

Although particle size distributions were fitted with log-normal distributions the nucleation mode size distributions are not symmetrical. Fig. 7 shows the typical evolution of the nucleation mode shape. At the beginning of the event (12:00), the nucleation mode is just a shoulder of the Aitken mode. Later on (13:30), the mode develops to its own peak, but the peak mean diameter is still below the detection limit. At 15:00, the nucleation mode mean diameter is above the detection limit, but small particles still form a shoulder for this peak, extending to sizes below the detection limit, indicating continuing particle formation. When the particle formation has finished at 23:00, the nucleation mode is quite log-normal. Before the build-up of the symmetrical mode, fitting the log-normal distribution might give strange results, especially at the beginning of the event when the maxima of the mode is below the detection limit.

During the particle production events, particle concentration did not increase equally at different heights. Inside the forest, the concentration was approximately half of the concentration above the forest during the strongest events. Above the forest, a concentration gradient was hardly distinguishable. The concentration gradient was visible just during fastest concentration increases. During these periods, the concentration was up to 5% higher on the 67-m level compared to the 18-m level. It seems that when the concentration changed, the 67-m level was first effected. Fig. 8 shows the production event on 2 April. The particle production event began just after noon. In the ratio between the 67-m level and 2-m level concentrations, up to 30% difference can be seen during the strongest concentration increase. During this event, the ratio between the 67-m and 18-m levels stayed very close to unity during daytime. During late evening, night and early morning, concentrations differ drastically because of the stable nocturnal surface layer. The forest seems to be a sink for small particles, although the condensating species might originate from the forest. Because the concentration changes were at first seen at the highest measurement level, particles seem not to be born near the canopy level.

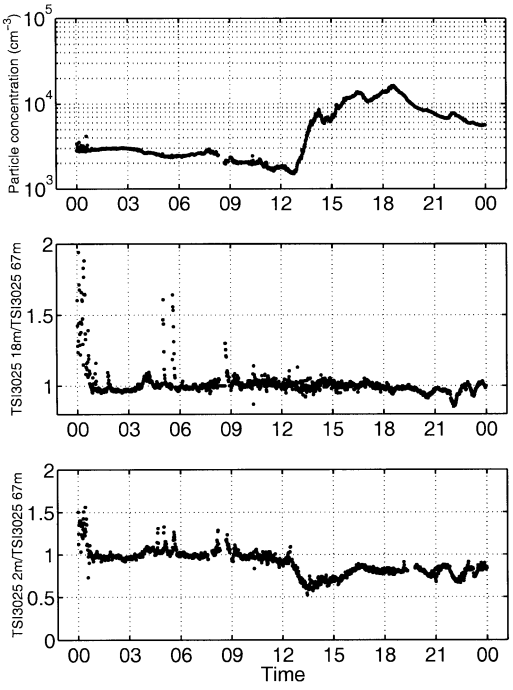

Fig. 8. Total concentration measured with TSI 3025 from 67-m level and the ratios of concentration on different levels during 2 April 1999.

If one studies the DMPS spectra from different levels, it easy to see that the sampling lines introduce sampling artifacts. Small particle concentrations at the 67-m level are significantly lower than that at the 2-m level (Figs. 9, 10). Also, the mean

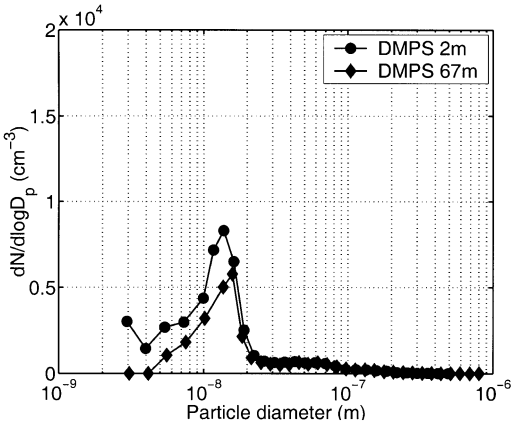

Fig. 9. Particle size distribution measured with DMPS from 2-m and 67-m levels at 2 April 1999 15:00.

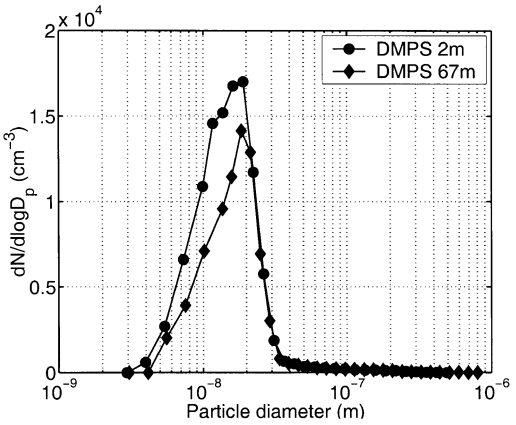

Fig. 10. Particle size distribution measured with DMPS from 2-m and 67-m levels at 2 April 1999 18:00.

size of the particle peak is larger at the 67-m level than at the 2-m level. However, particle growth rates measured during event days with the 67-m DMPS, are very close to the 2-m DMPS, despite the particle size discrepancy.

The concentration of particles between 3 and 10 nm can be calculated from the CPC pair total concentrations by subtracting the TSI 3010 concentration from TSI 3025 concentration. From the 2-m and 67-m DMPS measurements, this concentration can also be calculated. In Fig. 11, comparison between different instruments and measurement heights is presented. Concentrations calculated from the CPC pairs at different levels agree within $\pm 20\%$ during daytime. Because of the different cut sizes in the different CPCs, the small-particle concentrations at the 67- and 18-m levels do not track each other as well as total particle concentrations measured with the CPC pairs (Fig. 8). Around 12:00, the 18-m level has 20% more small particles than the 67-m level. Between 13:00 and 18:00, the concentration difference is less than 10%, but after that, the 67-m level concentration indicates up to twice more small particles compared to the 18-m level before 00:00. Concentrations calculated from DMPS measurements are much lower than those calculated from the CPC measurements. Compared to 67-m CPC values, the 2-m DMPS small-particle concentration is 40% lower than above the forest. The 67-m DMPS small-particle concentration is about half of the 2-m DMPS concentrations, due to the long sampling lines.

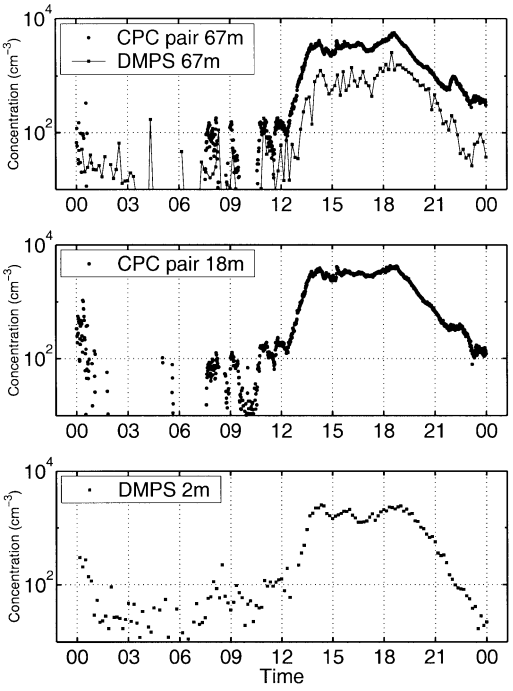

Fig. 11. Concentration of particles smaller than 10 nm on different levels 2 April 1999 calculated from DMPS and CPC pair measurements.

The PHAUCPC is also able to detect the small-particle concentration. We calculated the concentration of particles smaller than 6 nm for both PHAUCPC and DMPS at the 2-m level. This is not intended to be a direct comparison of the systems because at this time, no attempt had been made to invert the pulse-height distributions to obtain size distributions. Instead, concentrations are estimated directly from the pulse height distributions over nominal particle size ranges. This approach has the advantage of being straightforward, but it is known to underestimate nanoparticle concentrations. In this case, we estimate that it should underestimate concentrations by at most about a factor of 2. Surprisingly, the PHAUCPC small-particle concentration was just a fraction of those that DMPS was able to see (Fig. 12). The example shows the event during 14 April. During the beginning of the event, DMPS saw about 1000 particles smaller than 6 nm, when PHAUCPC saw less than 100 particles/cm^3. The total number concentration differed simultanously by less than 10% for the 2 instruments.

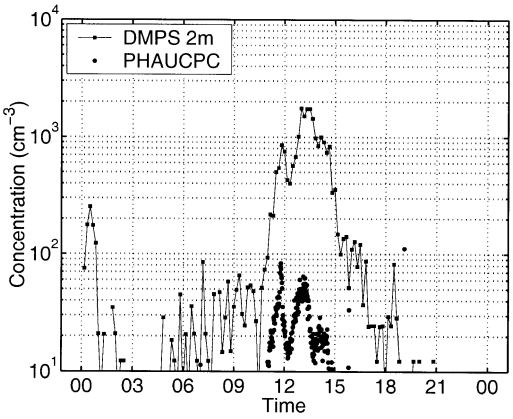

Fig. 12. Concentration of particles smaller that 6 nm calculated from PHAUCPC and DMPS measurements at 2-m level during 14 April 1999.

The fact that the PHAUCPC and DMPS total concentrations agree well, while the small-particle concentrations show significant concentration differences, is difficult to explain quantitatively. Nevertheless, it appears likely that the reason is related to the size calibration of the instruments. The size calibration for this work was done using standard methods widely used in aerosol research. These calibrations have been typically performed using silver (this study) or common inorganic salt particles (Saros et al., 1996; Stolzenburg, 1988; Wiedensohler et al., 1997; Porstendörfer and Soderholm, 1978). These particles generally do not interact with subsaturated organic vapours and their behaviour inside a CPC is similar (Saros et al., 1996). However, it is plausible that particles consisting largely of an organic fraction could form solution droplets with the butanol inside the CPC resulting in differing droplet activation and growth properties. If these particles reach larger sizes in the PHAUCPC than calibration aerosols, data analysis based on these calibrations would tend to underpredict the concentrations of 3–10 nm particles. Because the DMPS sizes particles based on electrical mobility and the CPC only measures particle concentration, the DMPS approach would not be sensitive to particle composition. Recent laboratory studies involving pure sulfuric acid particles measured with the PHAUCPC have shown that interactions between butanol and the sample particles can lead to differences in lower detection limit and droplet

sizes compared to calibrations using ammonium sulfate particles (Ball et al., 1999). Further laboratory studies are needed in order to confirm this hypothesis. However, the independent measurements of hygroscopic growth of ultrafine particles as well as the modeling of the particle growth processes indicate that there probably exists a large organic fraction of the new particle produced during the nucleation events (Hämeri et al., 2001; Kulmala et al., 2001).

The analysis of ion counter data revealed that bursts of intermediate and light large ions took place on 2, 4, 5, 6, 8, 9, 10, 12, 13, 14, and 19 April, overlapping with the periods when nucleation events were detected. An example of an ion burst event is presented in Fig. 13. The small ions have a diurnal pattern with rising small ion concentrations towards midday. The concentration of intermediate ions starts to rise at the same time as the CPC data show elevated particle concentrations due to the nucleation burst. Simultanous with the rising concentration of intemediate ions, there is a small dip in the small-ion concentration, which may be interpreted as an indication of a temporary small ion sink. It is difficult to say, based on these data, whether the small ion consumption occurs due to electrical charging of new neutral aerosol particles or due to ion-induced nucleation, removing ions from the small ion class. The light large ions display the burst 2–3 h later than intermediate ions.

The number concentration of the positive intermediate (ion size range of 1.9–7.4 nm), shown in Fig. 13, is roughly 160 cm^{-3} at maximum. Provided that steady state charging conditions for the sub-10-nm particles are obtained sufficiently rapidly after the nucleation, then the intermediate ions actually represent positively-charged aerosol particles. If a bipolar charging probability of 4% (Reischl et al., 1996) is assumed at 7 nm size, then the estimated total number concentration of these ultrafine particles rises to $\sim$4000 cm^{-3} at the maximum point. This exceeds the number concentration obtained from the CPC data and the DMPS data shown in Fig. 11. Furthermore, under a steady-state presumption, the agreement is already good for the light large ions (size range 7.4–20 nm). On the other hand, if the steady-state charging conditions are not assumed to be valid, this estimated excess of charged ultrafine particles would then possibly indicate a residual overcharge due to an ion-induced nucleation process. Additionally, we also lack more detailed size information on the intermediate ions within their own size class. It is very possible that particles in the size range of 2–3 nm may be responsible for the differences. This, however, would need interpretation of the disagreement in the size information from DMPS and PHAUCPC, shown in Fig. 12. All in all, we are not able to draw a final conclusion about the nucleation mechanisms based on these data.

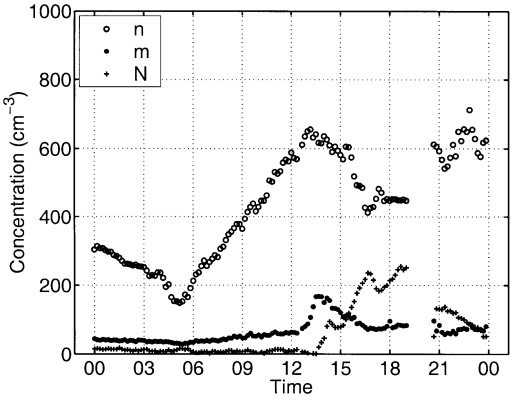

Fig. 13. Concentration of small (*n*; D_p less than 1.9 nm), intermediate (*m*; 1.9 nm $< D_p <$ 7.4 nm) and light large ions (*N*; 7.4 nm $< D_p <$ 20 nm) on 2 April 1999.

4. Conclusions

Measurements of the complete aerosol size distribution from 3 nm up to 20 μm were undertaken in the boreal forest environment. A number of particle measurement systems were required to cover such a range of sizes and a number of different approaches were required to examine particle concentrations at different sizes and at different locations. In general, reasonable agreement was achieved between most measurement systems; however, clear sampling artifacts did result which were impossible to correct for, highlighting the difficulties in undertaking such aerosol measurements.

Typically, the shape of the background distribution exhibited 2 dominant modes: a fine or Aitken mode with a mean diameter of 44 nm and a mean concentration of 1160 cm^{-3}, and an accumulation mode with mean size of 154 nm and a mean

concentration of 830 cm^{-3}. A coarse mode was also present, extending up to sizes of 20 μm having a number concentration of 1.2 cm^{-3}, volume mean diameter of 2.0 μm and a geometric standard deviation of 1.9. Total concentrations ranged from 410–45 000 cm^{-3}, the highest concentrations occurring on particle production days.

Particle production was observed on many days, typically occurring during sunny days in the late morning. Under these periods of new particle production, a nucleation mode was observed to form at sizes of the order of 3 nm and, on most occasions, this mode was observed to grow into Aitken mode sizes over the course of a day. The shape of the nucleation mode was quite log-normal after the actual particle production had eased. During production, new particles formed a shoulder to the nucleation mode extending to sizes below detection limit. Particle production was not detected when global radiation was less than 400 $W m^{-2}$ or when particle surface area was higher than 100 $\mu m^2 cm^{-3}$. During particle production days, SO_2 and NH_3 levels were higher than during other days when high surface area days were neglected. In southern air masses, small-particle concentrations were lower than in other air masses, because of higher surface area and increased cloudiness.

A clear gradient was observed between particle concentrations encountered below the forest canopy and those above, with significantly lower concentrations occurring within the canopy. Above the canopy, a slight gradient was observed between 18 m and 67 m, with a 5% higher concentration observed at 67 m during particle production days. Comparison of average size distributions for event and non-event days illustrates a less dominant accumulation mode, and consequently, a condensation sink, on event days when compared to non-event days.

5. Acknowledgements

The authors wish to thank Toivo Pohja for the installation work during the Biofor campaigns in Hyytiälä, and Aki Virkkula, and Risto Hillamo from the Finnish Meteorolgical Institute for providing the APS. This research has in part been supported also by the Estonian Science Foundation grants 3326 and 3903. The authors thank Aadu Mirme, Eduard Tamm, and Jaan Maasepp for their assistance at the preparation of air ion counters.

REFERENCES

Ball, S. M., Hanson, D. R., Eisele, F. L. and McMurry, P. H. 1999. Laboratory studies of particle nucleation: initial results for H_2SO4_4, H_2O, and NH_3 vapors. *J. Geophys. Res.* **104**, 23,709–23,718.

Birmili, W., Stratmann, F., Wiedensohler, A., Covert, D., Russell, L. M. and Berg, O. 1997. Determination of differential mobility analyzer transfer functions using identical instruments in series. *Aerosol Science and Technology* **27**, 215–223.

Covert, D. S., Kapustin, V. N., Quinn, P. K. and Bates, T. S. 1992. New particle formation in the marine boundary layer. *J. Geophys. Res.* **97**, 20,581–20,589.

Hämeri, K., Väkevä, M., Aalto, P., Kulmala, M., Swietlicki, E., Seidl, W., Becker, E. and O'Dowd, C. D. 2001. Hygroscopic and CCN properties of aerosol particles in boreal forests. *Tellus* **53B**, 359–379.

Hõrrak, U., Salm, J. and Tammet, H. 1998. Bursts of intermediate ions in atmospheric air. *J. Geophys. Res.* **103**, 13,909–13,915.

Hõrrak, U., Salm, J. and Tammet, H. 2000. Statistical characterization of air ion mobility spectra at Tahkuse Observatory: classification of air ions. *J. Geophys. Res.* **105**, 7,9291–9302.

Israël, H. 1970. *Atmospheric electricity* (Vol. I). Israël Program for Scientific Translations, Jerusalem.

Janson, R., Rosman, K., Karlsson, A. and Hansson, H.-C. 2001. Biogenic emissions and gaseous precursors to the forest aerosol. *Tellus* **53B**, 423–440.

Jokinen, V. and Mäkelä, J. M. 1997. Closed-loop arrangement with critical orifice for DMA sheath/excess flow system. *J. Aerosol Sci.* **28**, 643–648.

Kulmala, M., Rannik, Ü., Pirjola, L., Dal Maso, M., Karimäki, J., Asmi, A., Jäppinen, A., Karhu, V., Korhonen, H., Malvikko, S.-P., Puustinen, A., Raittila, J., Rommakkaniemi, S., Suni, T., Yli-Koivisto, S., Paatero, J., Hari, P. and Vesala, T. 2000. Characterization of atmospheric trace gas and aerosol concentrations at forest sites in southern and northern Finland using back trajectories. *Boreal Env. Res.* **5**, 315–336.

Kulmala, M., Hämeri, K., Aalto, P., Mäkelä, J. M., Pirjola, L., Nilsson, E. D., Buzorius, G., Rannik, Ü., Dal Maso, M., Seidl, W., Hoffmann, T., Jansson, R., Hansson, H.-C., O'Dowd, C., Viisanen, Y. and Laaksonen, A. 2001. Overview of the international project on biogenic aerosol formation in the boreal forest (BIOFOR). *Tellus* **53B**, 327–343.

Luts, A. and Salm, J. 1994. Chemical composition of small atmospheric ions near the ground. *J. Geophys. Res.* **99**, 10,781–10,785.

Mohnen, V. A. 1977. Formation, nature and mobility of ions of atmospheric importance. In: *Electrical processes in atmospheres* (ed. H. Dolezalek and R. Reiter). Dr. Dietrich Steinkopff Verlag, Darmstadt, Germany, 1–17.

Mäkelä, J. M., Aalto, P., Jokinen, V., Pohja, T., Nissinen, A., Palmroth, S., Markkanen, T., Seitsonen, K., Lihavainen, H. and Kulmala, M. 1997. Observations of ultrfine aerosol particle formation and growth in boreal forest. *Geophys. Res. Lett*. **24**, No. 10, 1219–1222.

Nilsson, E. D., Rannik, Ü., Buzorius, G., Boy, M. and Laakso, L. 2001. Effects of the continental boundary layer evolution, convection, turbulence and etntrainment on aerosol formation. *Tellus* **53B**, 441–461.

O'Dowd, C. D., Davison, B., Lowe, J. A., Smith, M. H., Harrison, R. M. and Hewitt, C. N. 1997. Biogenic sulphur emissions and inferred sulphate CCN concentrations in and around Antarctica. *J. Geophys. Res.* **102**, 12,839–12,854.

O'Dowd, C., McFiggans, G., Creasey, D. J., Pirjola, L., Hoell, C., Smith, M. H., Allan, B. J., Plane J. M. C., Heard, D. E., Lee, J. D., Pilling, M. J. and Kulmala, M. 1999. On the photochemical production of biogenic new particles in the coastal boundary layer. *Geophys. Res. Lett*. **26**, 1707–1710.

Pirjola, L., Laaksonen, A., Aalto, P. and Kulmala, M. 1998. Sulphate aerosol formation in the Arctic boundary layer. *J. Geophys. Res.* **103**, 8309–8322.

Porstendörfer, J. and Soderholm, S. C. 1978. Short Communication: Particle size dependence of a condensation nuclei counter. *Atmos. Envir*. **12**, 1805–1806.

Quant, F. R., Caldow, R., Sem, G. J. and Addison, T. J. 1992. Performance of condensation particle counters with three continous-flow designs. *J. Aerosol Sci.* **23**, S405–S408.

Reischl, G. P., Mäkelä, J. M., Karch, R. and Necid, J. 1996. Bipolar charging of ultrafine particles in the size range below 10 nm. *J. Aerosol Science* **27**, 931–949.

Saros, M. T., Weber, R. J., Marti, J. J. and McMurry, P. H. 1996. Ultrafine aerosol measurement using a condensation nucleus counter with pulse height analysis. *Aerosol Science and Technology* **25**, 200–213.

Stolzenburg, M. R. 1988. *An ultrafine aerosol size distribution measuring system*. PhD Thesis, University of Minnesota, Minneapolis MN, USA.

Stolzenburg, M. R. and McMurry, P. H. 1991. An ultrafine aerosol condensation nucleus counter. *Aerosol Science and Technology* **14**, 48–65.

Tammet, H. 1970. *The aspiration method for the determination of atmospheric-ion spectra*. Israël Program for Scientific Translations, Jerusalem.

Weber R. J., McMurry, P. H., Mauldin, R. L. III, Tanner, D. J., Eisele, F. L., Clarke, A. D. and Kapustin, V. N. 1999. New particle formation in the remote troposphere: a comparison of observations at various sites. *Geophys. Res. Lett*. **26**, 307–310.

Wiedensohler, A. 1988. An approximation of the bipolar charge distribution for the particles in the submicron size range. *J. Aerosol. Sci*. **19**, 387–389.

Wiedensohler, A., Covert, D. S., Swietlicki, E., Aalto, P., Heintzenberg, J. and Leck, C. 1996. Occurrence of an ultrafine particle mode less than 20 nm in diameter in the marine boundary layer during Arctic summer and autumn. *Tellus* **48B**, 213–222.

Wiedensohler, A., Orsini, D., Covert, D. S., Coffmann, D., Cantrell, W., Havlicek, M., Brechtel, F. J., Russell, L. M., Weber, R. J., Gras, J., Hudson, J. G. and Litchy, M. 1997. Intercomparison study of the size-dependent counting efficiency of 26 condensation particle counters. *Aerosol Science and Technology* **27**, 224–242.

Winklmayr, W., Reischl, G. P., Linder, A. O. and Berner, A. 1991. A new electromobility spectrometer for the measurement of aerosol size distributions in the size range 1 to 1000 nm. *J. Aerosol. Sci.* **22**, 289–296.